

# Low-Timing-Jitter and Low-Phase-Noise Microwave Signal Generation Using a VCSEL-Based Optoelectronic Oscillator

## Generación de señales microondas de bajo ruido y fluctuación de fase utilizando un oscilador

Christian Daniel Muñoz<sup>1</sup>, Juan Coronel<sup>2</sup>, Margarita Varón<sup>3</sup>, Fabien Destic<sup>4</sup>, and Angélique Rissons<sup>5</sup>

### ABSTRACT

This article presents the first results of the timing-jitter characterization of a VCSEL-based optoelectronic oscillator (VBO) at 2,5 GHz. For all implementations, vertical-cavity surface-emitting lasers (VCSEL) emitting in the O and C-bands were characterized. The resonant cavity was modified through the optical delay line length to verify its impact on timing-jitter and phase noise of the VBO. The lowest peak-to-peak jitter value obtained experimentally was 71 mUI when the optical fiber length was 1 km, whereas the lowest phase noise was -124 dBc/Hz with 5 km. This phase noise value, measured at 10 kHz offset, represents an 8 dB improvement compared to previous results, and it is the lowest value reported in the literature for the VBO architecture at 2,5 GHz.

**Keywords:** jitter, optoelectronic oscillator, phase noise, VCSEL, optical fiber

### RESUMEN

Este artículo presenta los primeros resultados de la caracterización de la fluctuación de fase (*jitter*) de un oscilador optoelectrónico basado en VCSEL (VBO) a 2,5 GHz. Para todas las implementaciones, se caracterizaron láseres de emisión superficial con cavidad vertical (VCSEL) que emiten en las bandas O y C. La cavidad resonante se modificó a través de la longitud de la línea de retardo óptico para verificar su impacto en la fluctuación temporal y el ruido de fase del VBO. El valor de *jitter* pico a pico más bajo obtenido experimentalmente fue 71 mUI cuando la longitud de la fibra óptica era de 1 km, mientras que el ruido de fase más bajo fue -124 dBc/Hz con 5 km. Este valor de ruido de fase, medido a 10 kHz de la portadora principal, representa un mejoramiento de 8 dB con respecto a resultados previos y es el valor más bajo registrado en la literatura para la arquitectura VBO a 2,5 GHz.

**Palabras clave:** fluctuación de fase, oscilador optoelectrónico, ruido de fase, VCSEL, fibra óptica

**Received:** May 11th, 2020

**Accepted:** August 5th, 2021

### Introduction

Nowadays, a wide range of applications, such as instrumentation (Wang *et al.*, 2020, Feng *et al.*, 2021), physical variable measurement (Zou *et al.*, 2016), and data transmission (Chi *et al.*, 2016), integrate electrical signals in the microwave and mm-wave range into their systems. Electronic oscillators have traditionally been used in telecommunications as high-frequency signal sources. However, the development of new and well-performing microwave signal generators is being boosted as a result of the emergence and evolution of some systems, e.g., radars and software-defined radio, as well as the use of higher frequencies in 5G (Ghosh *et al.*, 2019) and 6G cellular networks (Rappaport, Xing, Kanhere, Ju, Madanayake, Mandal, Alkhateeb and Trichopoulos, 2019). The systems based on optoelectronic components are a powerful alternative for microwave signal generation due to the high spectral purity that they can achieve (Sung *et al.*, 2007).

The optoelectronic oscillator (OEO) was developed in 1996 by Yao and Maleki (Yao and Maleki, 1996), and it is one

<sup>1</sup> Electronic Engineer, M.Sc. in Telecommunications Engineering, Universidad Nacional de Colombia, Colombia. Affiliation: Ph.D. candidate in Photonics and Optoelectronic Systems, ISAE-SUPAERO, Université de Toulouse, France. E-mail: 2cd.munoz@isae-supaero.fr

<sup>2</sup> Electronic Engineer, M.Sc. in Electrical Engineering, Universidad Nacional de Colombia, Colombia. Ph.D. Photonics and Optoelectronic Systems, ISAE-SUPAERO, France. Affiliation: Lead Laser Optics Researcher, Technology Innovation Institute, United Arab Emirates. E-mail: juan.coronel@tii.ae

<sup>3</sup> Electronic Engineer, Pontificia Universidad Javeriana, Colombia. M.Sc. in Optical Communications and Photonic Technologies, Politecnico di Torino, Italy. Ph.D. in Optoelectronics and Microwave, ISAE-SUPAERO, France. Affiliation: Full-Professor, Universidad Nacional de Colombia, Colombia. E-mail: gmvarond@unal.edu.co

<sup>4</sup> M.Sc. in Microwave and Optoelectronics, Université Paul Sabatier, France. Ph.D. Photonics and Optoelectronic Systems, ISAE-SUPAERO, France. Affiliation: Research Engineer, ISAE-SUPAERO, Université de Toulouse, France E-mail: f.destic@isae-supaero.fr

<sup>5</sup> Degree in Physics-Chemistry, Université de Reims, France. M.Sc. and Ph.D. in Optoelectronics and Microwave, ISAE-SUPAERO, France. Affiliation: Full-Professor, ISAE-SUPAERO, Université de Toulouse, France. E-mail: a.rissons@isae-supaero.fr

**How to cite:** Muñoz, C. D., Coronel, J., Varón, M., Destic, F., and Rissons, A. (2022). Low-timing-jitter and Low-Phase-Noise Microwave Signal Generation Using a VCSEL-Based Optoelectronic Oscillator. *Ingeniería e Investigación*, 42(2), e87189. <http://doi.org/10.15446/ing.investig.v42n2.87189>



Attribution 4.0 International (CC BY 4.0) Share - Adapt

of the most sophisticated mechanisms for the generation of spectrally pure microwave signals (low phase noise). One of the main advantages of the OEO architecture is its high configuration flexibility, *i.e.*, it can be implemented in a wide variety of versions with different optical and electrical components in order to optimize its performance. In this topology, the cavity is an optical fiber delay line, and its length is related to the phase noise and the space between different non-oscillating modes. By increasing the optical fiber length, the phase noise decreases, but, at the same time, the mode spacing decreases. Multi-loop oscillators include several parallel delay lines into the cavity to guarantee an acceptable phase noise and a large mode spacing (Chen *et al.*, 2015).

In the OEO architecture proposed by Yao and Maleki (1996), the laser source is externally modulated through an intensity modulator driven by the generated microwave signal. The VCSEL-based optoelectronic oscillator (VBO) was introduced in 2006 (Varón *et al.*, 2006), and its architecture includes a directly modulated VCSEL. This type of laser, known for its low power consumption and low cost, is suitable for embedded aerospace applications (Rissons *et al.*, 2012). In addition to the advantages of VCSEL lasers, the implementation of VBOs is less expensive, smaller, and requires a smaller operating current than other implementations. The VCSEL bandwidth determines the highest oscillating frequency, and some authors have achieved frequencies up to 10 GHz with phase noises of -80 dBc/Hz (Hasegawa *et al.*, 2007) and -70 dBc/Hz (Koizumi *et al.*, 2010) at 10 kHz from the carrier.

The frequency stability of a clock or a microwave signal can be estimated through single-sideband (SSB) phase noise and jitter measurements (IEEE, 2021). On the one hand, phase noise is a frequency domain measurement of phase deviations that allows identifying some of the noise sources within the system (Rubiola, 2008). On the other hand, jitter is the time deviation of an event (usually the rise or fall event in digital systems and clocks) from an ideal reference time frame or sampling point (Da Dalt and Sheikholeslami, 2018). In digital transmission systems, increasing transfer rates are limited by mistiming in regeneration processes (Ryu *et al.*, 2020). For this reason, ultra-low jitter clocks must be implemented to meet the tolerance ranges of transmitting and receiving equipment (Choi *et al.*, 2019).

Some transmission systems such as optical transport networks (OTN) and Gigabit Ethernet networks include precise specifications regarding jitter tolerance and frequency accuracy (ITU, 2018). In this way, the application of an optoelectronic oscillator in a digital data transmission system can be established through jitter and phase noise measurements. As a contribution to this field, we present the first timing-jitter analysis for a VCSEL-based optoelectronic oscillator. The VBO implementation of this work uses the latest generation of VCSELs in the O and C-bands with reduced relative intensity noise (RIN) in comparison to VCSELs used in previous publications (Varón *et al.*, 2006; Rissons *et al.*, 2012; Koizumi *et al.*, 2009).

This paper is structured as follows: the first section comprises a detailed VCSEL description and an experimental laser characterization for both VCSELs used; then, the VBO architecture is described, and a phase noise predictive model is presented; the VBO implementation, in terms of phase noise and timing-jitter, is addressed in a third section; some performance comparisons between our systems and previous VBO implementations available in the literature are detailed in the fourth section; and, finally, the last section presents some conclusions about our work.

## Vertical-cavity surface-emitting lasers -VCSEL

The vertical-cavity surface-emitting lasers are semiconductor lasers widely used in telecommunications at high transfer rates through different modulation formats, such as direct modulation (Malacarne *et al.*, 2017), discrete multitone modulation (DMT) (Wagner *et al.*, 2017) and four-level pulse amplitude modulation (PAM-4) (Lavernick *et al.*, 2017). While multimode VCSELs at short-wavelengths (850 - 1 050 nm) are employed in short-reach fiber links (Pavan, Lavrencik and Ralph, 2017) and visible light transmissions (Li-Fi) at 680 nm (Lu *et al.*, 2017), long-wavelength VCSELs (LW-VCSEL) in the 1,2 -1,6  $\mu\text{m}$  range, are used in long-haul communications (Bacou *et al.*, 2010).

The development of LW-VCSELs has evolved in recent years according to their requirements and applications. Wafer-fused LW-VCSEL technology is the most applied for VCSEL manufacturing, covering the entire ITU-T single-mode spectral range (1 260 nm - 1 675 nm). The main drawback of this technology is the integration of the active region (which requires high optical gain) with the mirrors (high-reflectivity, low optical absorption, and high thermal conductivity) in a monolithic semiconductor (Belkin *et al.*, 2015).

VCSEL manufacturing has three particularities. First, the active cavity is grown on an InP substrate and incorporates InAlGaAs quantum wells (QW) covering both bands (Syrbu *et al.*, 2005). Secondly, the top and bottom AlGaAs/GaAs distributed Bragg reflectors (DBRs) are bonded to the active cavity using localized wafer fusion (Iakovlev *et al.*, 2005). This approach avoids VCSEL overheating problems. Finally, tunnel junctions (TJ) are grown to reduce free carrier absorption and mirror optical loss, as well as to ensure a single-mode transverse emission (Belkin *et al.*, 2015).

The O and C-band VCSELs used for this work were produced by the Korean manufacturer RayCan, and their structure is depicted in Figure 1. All layers were epitaxially grown by metal-organic chemical vapor deposition (MOCVD) on InP substrate (Park *et al.*, 2006). Each laser was placed inside a TO-56 package, and its output beam was coupled to a single-mode optical fiber.

The optical power versus bias current for both VCSELs is presented in Figure 2. The maximum emission powers of O and C-band VCSELs are 0,97 mW and 0,89 mW when the

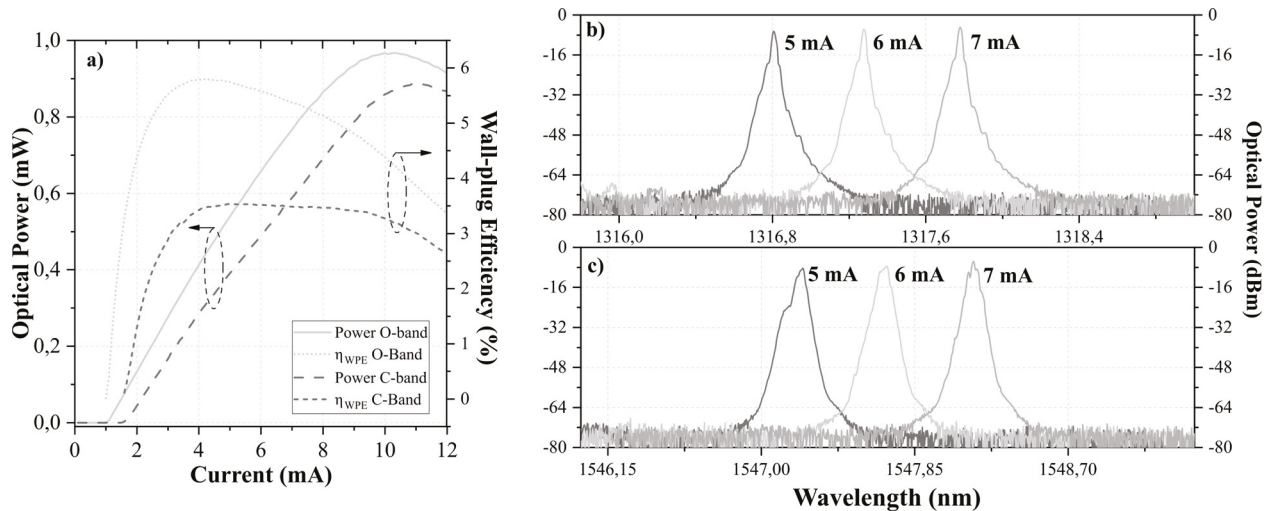


**Figure 2.** a) Bias current vs. output power and wall-plug efficiency (optical spectra at 5, 6 and 7; mA b) O-band c) C-band VCSEL  
**Source:** Authors

bias currents are 10,3 mA and 11,1 mA, respectively. The reduced threshold currents are close to each other (1 mA for O-band and 1,5 mA for C-band) and represent 10% of the current for a distributed feedback laser (DFB).

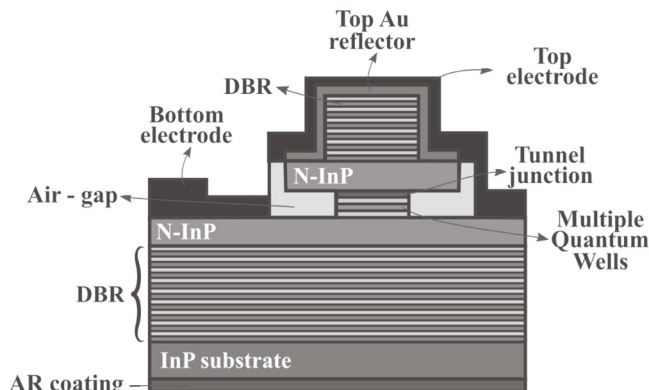


**Figure 1.** Cross-sectional VCSEL structure  
**Source:** Adapted from (Park et al., 2006)

The selected bias current for the VBO implementations was 6 mA, given the linearity in this region, the constant wall-plug efficiency (WPE) after 4 mA, and the linear behavior of the dynamic resistance. Figure 2 shows the single-mode operation of VCSELs at different bias current and wavelengths around 1,31  $\mu\text{m}$  and 1,54  $\mu\text{m}$ .

Another relevant parameter for the VBO implementation is the relative intensity noise (RIN) due to its influence on the oscillator phase noise. RIN is expressed in dB/Hz and relates the photon density fluctuation to the mean photon square density. RIN measurements at 25 °C for both VCSELs are shown in Figure 3. Regardless of the optical band, the RIN decreases when the bias current increases, since the stimulated emission is higher than the spontaneous one when the bias current moves away from the threshold current. Under the same conditions, and considering the RIN

values at 2,5 GHz, the RIN is slightly lower in the O-band VCSEL for all bias currents. The RIN values for 5, 6 and 7 mA are -141, -144 and -146,5 dB/Hz, respectively, whereas, for the C-band VCSEL, they are -138, -142 and -143 dB/Hz. Considering the experimental results and the measurement uncertainty, both lasers impact the phase noise in the same proportion.

## VCSEL-based optoelectronic oscillator

The VCSEL-based optoelectronic oscillator (VBO), which is illustrated in Figure 4, is a self-seeding ring oscillator composed of a directly modulated VCSEL that passes through a low-loss glass fiber, which acts as an optical delay line. Owing to the lower attenuation, long cavity length and a high-quality factor Q are possible, thus allowing low phase noise. Then, the optical signal is converted to the electrical domain by a photodetector. The electrical signal is amplified by a microwave amplifier to compensate loop losses and then filtered by a band-pass filter to select the oscillation frequency and remove the spur modes. Finally, the loop is closed using an electrical coupler, which allows extracting the generated microwave signal (Hayat et al., 2008).

The selectivity of the oscillation mode will depend on the resonant element through the optical delay  $\tau_d$  produced by the optical fiber. The quality factor for the VBO is directly proportional to the optical fiber length, and it is expressed as follows:

$$Q = 2\pi f\tau_d \quad (1)$$

The oscillation mode is selected from the optical fiber frequency comb by the microwave band-pass filter. The mode spacing in the optical fiber is defined as the free spectral range (FSR), which is expressed as:

$$FSR = \frac{c}{n_f L} \quad (2)$$

where,  $c$  is the speed of light,  $n_f$  is the refractive index of the optical fiber core, and  $L$  is the optical fiber length. The longer the optical fiber, the closer the optical fiber oscillation modes. The selected mode lies inside the microwave filter band-pass bandwidth.

VBO phase noise is related to the phase fluctuation propagation of optical and electrical components inside the loop. By using Rubiola's linear feedback approach for delay-line oscillators (2008), the power spectral density (PSD) of phase fluctuations  $S_\phi(s)$  can be expressed as follows:

$$S_\phi(j\omega) = \left| \frac{1}{1+B(j\omega)} \right|^2 (S_\psi(j\omega) + S_{amplifier}(j\omega)) \quad (3)$$

where  $B(j\omega)$  is the transfer function of the resonator and the delay line,  $S_\psi(j\omega)$  is the noise power spectral density due to components, and  $S_{amplifier}(j\omega)$  the microwave amplifier noise. The main noise contributions from the components are the phase variation in the optical fiber, the thermal and shot noise, and the relative intensity noise of VCSELs. By definition, phase noise is the half of the one-sided PSD of phase fluctuations (IEEE, 2009); thus, the VBO phase noise  $L(f)$  can be expressed as follows:

$$L(f) = \left( \left| \frac{1}{1+B(j\omega)} \right|^2 (S_\psi(j\omega) + S_{amplifier}(j\omega)) \right) / 2 \quad (4)$$

Another useful metric to verify frequency stability is timing-jitter, which corresponds to the short-term temporal variations of a signal relative to an ideal signal (International Telecommunication Union (ITU), 1996). Although phase noise is a frequency domain measurement and jitter is a time-domain measurement, both are related through Equation (5) (Da Dalt and Sheikholeslami, 2018):

$$\sigma_{RMS} = \frac{1}{2\pi f_c} \sqrt{2 \int_{f_{min}}^{f_{max}} L(f) df} \quad (5)$$

where  $\sigma_{RMS}$  corresponds to the root mean squared (RMS) jitter,  $f_c$  is the oscillation frequency, and  $f_{min}$  and  $f_{max}$  are the lower and upper frequency of the phase noise measurement, respectively. Jitter measurements can be composed of two individual contributions: random and deterministic jitter. On the one hand, random jitter (RJ) is caused by uncorrelated noise, e.g., thermal noise. Moreover, it generally follows a normal or Gaussian distribution. On the other hand, deterministic jitter (DJ) comes from systematic effects (intersymbol interference (ISI) and periodic jitter), and it can be predicted and reduced.

## 2,5-GHz VCSEL-based optoelectronic oscillator characterization

### Setup description

Several VBOs at 2,5 GHz using 1,31  $\mu\text{m}$  and 1,54  $\mu\text{m}$  VCSELs were implemented and characterized through phase noise and jitter measurements. As stated before, the goal of using a direct modulated VCSEL is to develop a high spectral purity oscillator with low power consumption. For this oscillator, a cavity band-pass filter centered at 2,5 GHz, 3 MHz bandwidth at 3 dB, and insertion losses lower than 3 dB is used. A 39 dB gain low noise microwave amplifier is used to amplify the selected mode. The amplifier output is connected to a tunable attenuator in order to control the closed-loop gain, and the output is then connected to a bias tee to modulate the optical source.

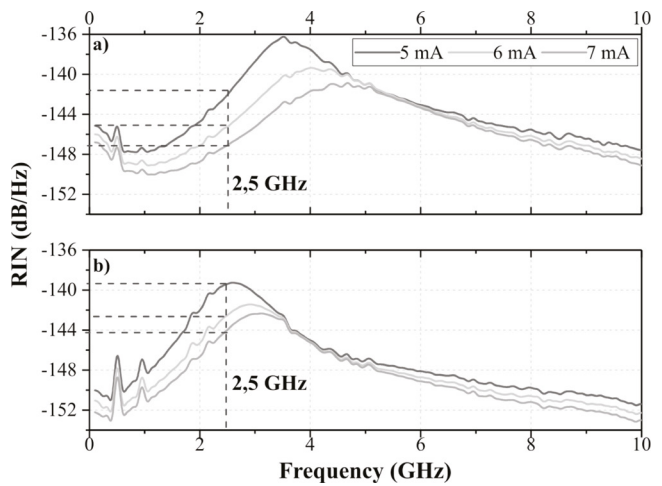


Figure 3. RIN measurements at 25 °C: a) O-band, b) C-band VCSEL Source: Authors

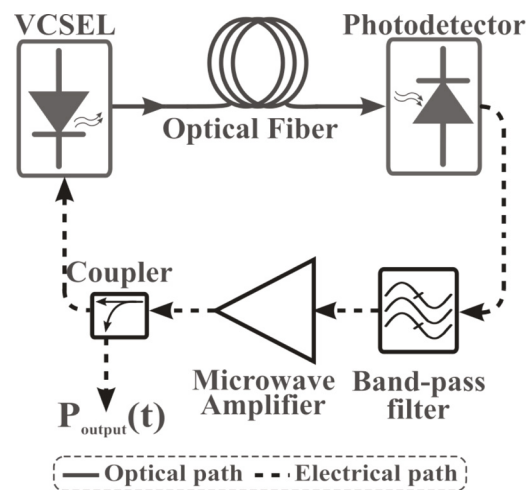


Figure 4. VCSEL based optoelectronic oscillator setup Source: Adapted from (Hayat et al., 2008)

The optical fiber length is varied from 1 to 5 km in order to evaluate its effects on spectral purity and jitter variations. The measured and calculated FSR for each length are presented in

**Table 1.** Although a higher Q factor guarantees lower phase noise values, the reduced FSR can directly impact some sensitive parameters for telecommunications applications, such as jitter and residual phase modulation (PM), through the contribution of each non-oscillating mode.

### Electrical output spectrum

**Figure 5** shows the electrical spectrum taken from a 20-dB coupler output for 1 km. The measured FSR is 190 kHz, and the difference with the theoretical value corresponds to the fiber length uncertainty and the delay contribution of the electronic components. The oscillation power is -10 dBm, and the side mode suppression ratio (SMSR) to the first non-oscillating mode is 59 dB. The oscillation power can be improved by using an electrical coupler with a less attenuated output.

**Table 1.** Measured and calculated FSR values for several fiber lengths

Fiber length (km)	Calculated FSR (kHz)	Measured FSR (kHz)
1	204	190
2	102	98
3	68	65
5	41	40

Source: Authors

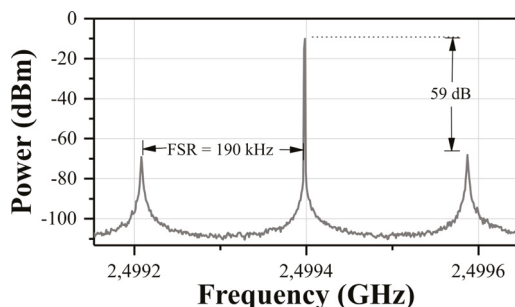


**Figure 5.** 2,5 GHz VCSEL-based optoelectronic oscillator output spectrum

Source: Authors

### Phase noise characterization

The phase noise measurements for each VBO configuration are taken using a direct measurement method through an electrical spectrum analyzer ESA (R&S FSW50). For measurement validation purposes, a calibrated phase noise signal is implemented through frequency modulation (FM) of an ultra-low phase noise source (at 2,5GHz) with uniform noise (Gheen, 2012). According to the difference between the technical specifications of the ultra-low phase noise source and the phase noise measurements, the lowest of the latter, using direct method, is limited to -130 dBc/Hz at 10 kHz from the carrier.

**Figure 6** shows the phase noise curves of the implemented VBOs using O and C-band VCSELs. In both cases, the phase noise is improved when the optical fiber delay line is enlarged, i.e., when the quality factor of the resonator is increased.

Additionally, the phase noise level difference between the optical bands is given by the zero chromatic dispersion of the standard single-mode optical fiber employed at 1,3  $\mu\text{m}$ . In this sense, the lowest phase noise values are achieved when a O-band VCSEL is used.

Regardless the optical fiber length, two noise processes are identified in the phase noise curves. The white phase noise process is located far from the carrier (from 20 kHz), and it is produced mainly by the white noise of the microwave amplifier. On the other hand, the white frequency noise process varies at a -20 dB/decade rate, and it results in the up-conversion process (also called Leeson effect) from the flicker noise of the amplifier inside the loop (Guo *et al.*, 2018). For the O-band VCSEL, white frequency noise is present in the two first decades (from 100 Hz to 10 kHz); for the C-band, the same slope is located only from 2 kHz to 10 kHz. In this decade, the slope becomes -25 dB/decade due to a more significant RIN contribution in this band.

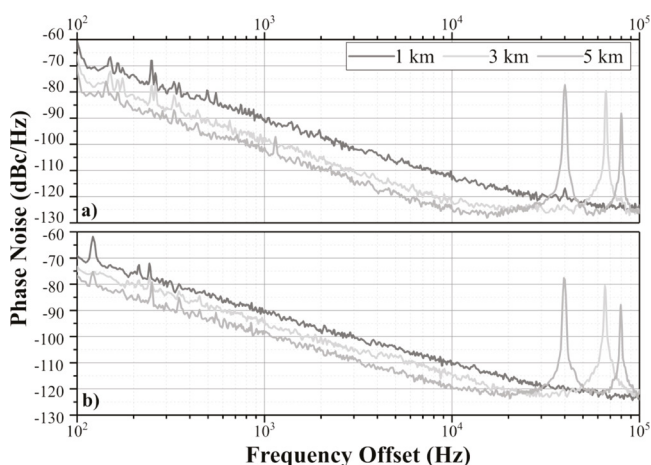


**Figure 6.** Phase noise curves for: a) O-band VCSEL, b) C-band VCSEL

Source: Authors

### Timing-jitter characterization

For the phase noise curves using 3 and 5 km, the sharp peaks are spaced at 65 and 40 kHz, respectively. These values correspond to the FSR values summarized in Table 1. The frequency comb peaks are close to each other and cannot be rejected by the microwave band-pass filter. Consequently, these non-rejected peaks become secondary oscillation modes that can increase the timing-jitter. Figure 7 depicts the histograms (10 000 samples) of the time interval error (TIE) measurement using an O-band VCSEL and different fiber lengths.

In all cases, the histograms show a dominant Gaussian behavior, i.e., the main contribution comes from random jitter. The TIE RMS jitter was determined through the standard deviation of the Gaussian distribution of each histogram. Contrary to what was expected, the TIE RMS jitter increases as the fiber length increases. This phenomenon has two reasons. Firstly, the new non-rejected modes expand the profile of the Gaussian distribution due to additional periodic

jitter. Secondly, the amplifier input power decreases due to the higher optical attenuation, and, consequently, the white noise contribution of the amplifier is stronger. One way to reduce this effect is to use a band-pass filter with narrower bandwidth, therefore reducing the contribution of periodic jitter of each mode. Table 2 summarizes the measured phase noise at 10 kHz offset and the peak-to-peak jitter expressed in unit interval (UI) for each case.

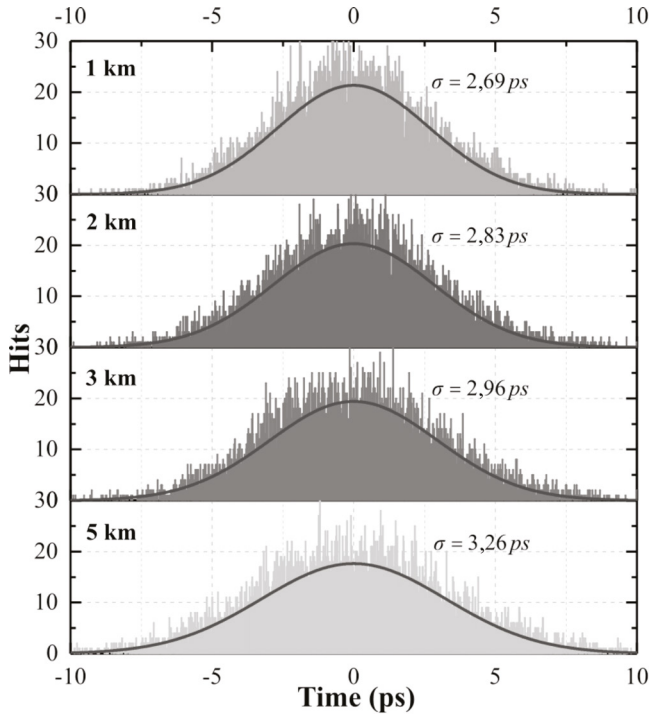


**Figure 7.** Jitter histograms of VBO using O-band VCSEL  
Source: Authors

According to Table 2, and under the same conditions, the lowest phase noises and jitters are obtained using O-band VCSELs. This effect is mainly due to the zero-dispersion of the fiber at wavelengths close to 1,3  $\mu\text{m}$  and the level power inside the loop. For both lasers, the phase noise improves proportionally when the resonator length increases, but, at the same time, the jitter deteriorates. Although the peak-to-peak jitter increases from 71 to 106 mUI, in any case, the values exceed the specifications of local clocks for OTN networks defined by the recommendation ITU-T G.8251 (ITU, 2018).

**Table 2.** VBO phase noise and peak-to-peak jitter

Fiber length (km)	Phase Noise (dBc/Hz) Oband	PkPk jitter (mUI) Oband	Phase Noise (dBc/Hz) Cband	PkPk jitter (mUI) Cband
1	-113,5	71	-110	88
2	-117	81	-112,8	91
3	-121,7	84	-114,5	95
5	-124,8	95	-119	106

Source: Authors

### Phase noise model validation

The linear model of Equation 4 allows estimating the phase noise of the VBO considering different noise sources. The transfer function  $B(j\omega)$  is determined using the Laplace transform to the phase impulse response of the optical delay ( $B_o(j\omega) = e^{-j\omega\tau_d}$ ) and the microwave filter ( $B_f(j\omega) = 1/(1 + j\omega\tau_f)$ ), where  $\tau_f$  is the filter group delay. The noise power spectral density  $S_\psi(j\omega)$  referred to the input impedance of the amplifier ( $Z_A$ ) includes all the additive noise sources inside the loop (VCSEL RIN at the oscillating frequency  $RIN_{VCSEL}$ , shot and thermal noise, and the intensity-to-phase noise conversion process due to Rayleigh scattering  $RIN_{fiber}$ ).  $S_\psi(j\omega)$  can be expressed as:

$$S_\psi(j\omega) \left[ \left( RIN_{VCSEL} + RIN_{fiber} \right) i_{ph}^2 + 2qi_{ph} + \frac{4k_B T}{R_{ph}} \right] * Z_{ph} \parallel Z_A \quad (6)$$

where  $i_{ph}$  is the photodetected current,  $k_B$  is the Boltzman constant,  $T$  is the operating temperature, and  $Z_{ph}$  is the photodetector impedance. The power spectral density of the microwave amplifier  $S_{amplifier}(f)$  involves white noise and flicker noise (Rubiola, 2008). The white noise component is estimated from the equivalent noise spectral density ( $N = FkT_0$ ) and the carrier power  $P_0$  at the amplifier input (Rubiola and Giordano, 2007). In contrast, flicker noise is independent of carrier power at the amplifier input over a wide frequency range. Hence,  $S_{amplifier}(f)$  corresponds to:

$$S_{amplifier}(f) = b_0 + \frac{b-1}{f} = \frac{FKT_0}{P_0} + \frac{b-1}{f} \quad (7)$$

where  $b_{-1}$  is a constant coefficient of flicker noise,  $F$  is the noise figure, and  $kT_0$  is the thermal energy.

Figure 8 presents the estimated phase noise curves using the electrical power  $P_{or}$  which was experimentally obtained, and the technical characteristics of loop components summarized in Table 3. Figure 8a presents the estimated phase noise when the fiber length is 1, 2, 3, and 5 km, and the amplifier input power is constant. The phase noise at 10 kHz offset is reduced by 12 dB from -116,8 dBc/Hz to -128 dBc/Hz when the length is 1 km and 5 km, respectively. The estimated phase noise curves when  $P_0$  ranges from -50 dBm to -35 dBm are plotted in Figure 8b. As expected, the input power modified the floor phase noise and the noise level far from the carrier. Therefore, the phase noise at 10 kHz from the carrier is improved by 14 dB (from -117,2 dBc/Hz to -131,5 dBc/Hz). The noise close to the carrier is also reduced, but it is limited by the additive noise sources and the flicker noise coming from the microwave amplifier. The level difference between the estimated and measured phase noise is caused by measurement uncertainty (around 3 dB for the direct method) and because some parameters are assumed from the literature.

The effect of the VCSEL RIN on the phase noise is represented in Figure 8c by assuming three different noise values: -120, -130, and -140 dB/Hz. For values below -130 dB/Hz, the phase noise at 10 kHz from the carrier is slightly enhanced (2 dB better when RIN = -140 dB/Hz). Conversely, when the RIN is -120 dB/Hz, the phase noise deteriorates rapidly by 8 dB from the value obtained for RIN = -130 dB/Hz (-116,64 dBc/Hz).

The RMS jitter can be also estimated by employing Equation 5 and the phase noise curves plotted in Figure 8a. By lengthening the optical fiber from 1 to 5 km, the RMS jitter is reduced from 1,37 ps to 0,33 ps, respectively. The difference between the estimated RMS jitter and the TIE jitter measurements is given by the aliasing and the noise floor of the oscilloscope used for the measurements.

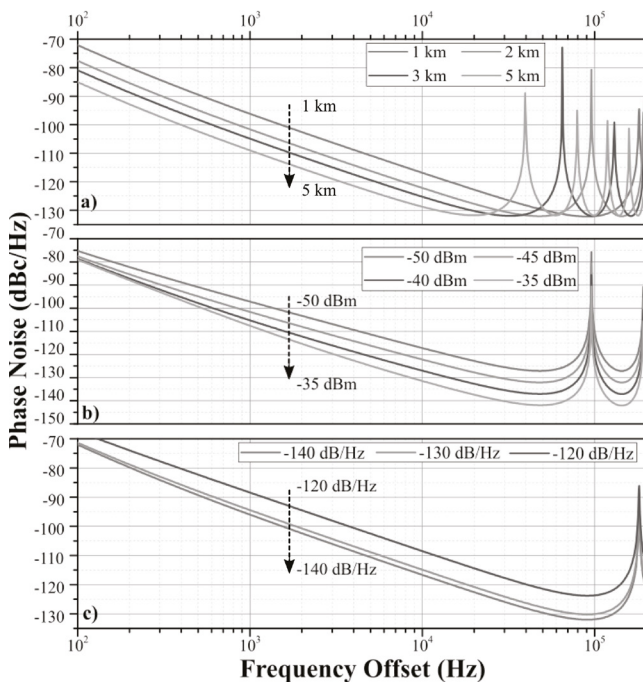


**Figure 8.** Phase noise simulation using different a) optical fiber lengths, b) amplifier input powers, and c) RIN values  
**Source:** Authors

**Table 3.** Parameters used to estimate the theoretical phase noise

Parameter	Value
RIN @2,5 GHz	-140 dB/Hz
$Z_{ph}$	100 $\Omega$
$Z_A$	50 $\Omega$
$P_o$	-48 dBm
$F$	3 dB
$T_o$	25 $^{\circ}$ C
$b-1$	-100 rad <sup>2</sup> /Hz

**Source:** Authors

## Performance comparison

Table 4 presents some phase noise results obtained by different authors using short and long-wavelength VCSELs.

In all cases, the oscillating frequency is limited by the bandwidth laser and the electrical access. At 2,49 GHz, the highest phase noise is -100 dBc/Hz, and it was obtained when a multimode VCSEL emitting at 0,85  $\mu$ m and 120-m optical fiber were employed. Despite the reduced RIN of the multimode VCSEL (-130 dB/Hz), the phase noise of the VBO was deteriorated by the high attenuation and the reduced Q-factor provided by the multimode optical fiber.

When long-wavelength VCSELs are used, the phase noise of the generated microwave signal is improved in all cases. This event is mainly attributed to the RIN reduction resulting from the technological advances in VCSEL manufacturing, as well as the lengthening of single-mode optical fiber.

The lowest phase noise values of our work were obtained when the optical fiber length was 5 km. The phase noises were -124,8 dBc/Hz and -119 dBc/Hz when the emitting wavelengths were in the O and C-bands, respectively. To the best of our knowledge, these values are the lowest reported in the bibliography at 2,5 GHz when direct modulation is applied. According to the numerical results presented in the previous section and the experimental results (Table 4), we attribute the phase noise improvement to the reduction of the white phase noise through the amplifier input power  $P_o$ , and the lengthening of the optical fiber.

## Conclusions

This paper presents the first time-domain stability characterization of several VBO implementations by performing timing-jitter measurements and their frequency-domain stability through phase noise measurements. As stated, both stability measurements are frequently used for establishing clock accuracy for several data transmission systems.

For all the experimental validations, the last generation of O and C-band VCSELs with reduced RIN levels were employed. In this way, VCSEL RIN and longer optical fiber have improved the phase noise by 8 dB in comparison with previously reported results. The best phase noise performance measured at 10 kHz from the carrier was -124,8 dBc/Hz, and it corresponds to the lowest value reported in the literature for a 2,5 GHz-VBO. It was experimentally demonstrated that the longer the optical fiber, the better the spectral purity, but, at the same time, the worse the timing-jitter deterioration. According to the application, a trade-off must be made between phase noise and timing-jitter.

Given the higher contribution from the non-oscillation modes, the peak-to-peak jitter increases from 71 to 106 mUI when the optical fiber length is enlarged from 1 to 5 km. In all cases, the electrical output of the VBO can be used as a recovery clock that meets the jitter tolerances of ITU-T G.813 for STM-16 transmissions and Telcordia GR-253-CORE for OC-48 transmissions.

**Table 4.** VCSEL based optoelectronic oscillator performance comparison

Reference	Laser wavelength ( $\mu\text{m}$ )	Frequency (GHz)	Phase noise (dBc/Hz)	Optical fiber length (m)
(Varón et al., 2006)	0,85	2,49	-100	120
(Hayat et al., 2008)	1,3	2,49	-107,5	1 000
(Rissons et al., 2012)	1,3	2,49	-116	2 000
(Belkin et al., 2015)	1,3	3	-106	65
This work (2020)	1,3	2,5	-124,8	5 000
This work (2020)	1,5	2,5	-119	5 000

**Source:** Authors

The phase noise estimation model agrees with the experimental characterization of the far-from-the-carrier microwave signal. The model can be improved by a complete characterization of the microwave amplifier and the addition of multiplicative noise sources such as the frequency noise and the low-frequency RIN of the VCSEL.

Considering the good phase noise performance and its lower power consumption, the VBO is suitable for embedded applications and an all-integrated solution can be explored. Additionally, high-bandwidth on-chip VCSELs can be employed to increase the oscillating frequency.

For future developments, it is recommended to employ other resonant elements such as fiber ring resonators, whispering gallery modes, or double feedback loop oscillator in order to explore the spectral purity performance in the frequency domain. A stability analysis in the time domain (long-term stability) is proposed, which uses a deviation.high-resolution frequency counter and the Allan standard deviation.

## Acknowledgements

The authors would like to thank COLCIENCIAS and the French Ministry of Higher Education for funding the mobility and exchange of the researchers through the projects M301PR03F18 and C17P01, as well as the Departmental Government of Nariño for supporting this work through grant No. BPIN 2013000100092.

## References

Bacou, A., Hayat, A., Iakovlev, V., Syrбу, A., Rissons, A., Mollier, J., and Kapon, E. (2010). Electrical modeling of long-wavelength VCSELs for intrinsic parameters extraction. *IEEE Journal of Quantum Electronics*, 46(3), 313-322. <https://doi.org/10.1109/JQE.2009.2031312>

Belkin, M.-E., Belkin, L., Loparev, A., Sigov, A.-S., and Iakovlev, V. (2015). Long wavelength VCSELs and VVCSEL-based processing of microwave signals. *IntechOpen*. <https://doi.org/10.5772/60480>

Chen, H., Xia, M., Sun, M., and Sun, X. (2015). A high-speed tunable optoelectronic oscillator with a fine step based on semiconductor optical amplifier. *Microwave and Optical Technology Letters*, 57(2), 464-467. <https://doi.org/10.1002/mop.28868>

Chi, Y.-C., Lin, G.-R., Chi, Y., and Lin, G. (2016). Optoelectronic oscillators. In J. G. Webster (Ed.) *Wiley Encyclopedia of Electrical and Electronics Engineering* (pp. 1-2). John Wiley & Sons. <https://doi.org/10.1002/047134608X.W8304>

Choi, S., Yoo, S., Lee, Y., Jo, Y., Lee, J., Lim, Y., and Choi, J. (2019). An ultra-low-jitter 22.8-GHz ring-LC-hybrid injection-locked clock multiplier with a multiplication factor of 114. *IEEE Journal of Solid-State Circuits*, 54(4), 927-936. <https://doi.org/10.1109/JSSC.2018.2883090>

Da Dalt, N. and Sheikholeslami, A. (2018). *Understanding jitter and phase noise: A circuits and systems perspective*. Cambridge University Press. <https://doi.org/10.1017/9781316981238>

Feng, D., Gao, Y., Zhu, T., Deng, M., Zhang, X., and Kai, L. (2021). High-precision temperature-compensated magnetic field sensor based on optoelectronic oscillator. *Journal of Lightwave Technology*, 39(8), 2559-2564. <https://doi.org/10.1109/JLT.2021.3050153>

Gheen, K. (2012). *Phase noise measurements methods and techniques, technical report application note*. Agilent Technologies.

Ghosh, A., Maeder, A., Baker, M., and Chandramouli, D. (2019). 5g evolution: A view on 5g cellular technology beyond 3GPP release 15. *IEEE Access*, 7, 127639-127651. <https://doi.org/10.1109/ACCESS.2019.2939938>

Guo, J.-J., Jin, X.-D., Zhu, Y.-H., Jin, X.-F., Chi, H., Zheng, S., and Zhang, X. (2018). A comprehensive model for phase noise characteristics of an optoelectronic oscillator. *Microwave and Optical Technology Letters*, 60(9), 2194-2197. <https://doi.org/10.1002/mop.31327>

Hasegawa, H., Oikawa, Y., and Nakazawa, M. (2007). A 10-ghz optoelectronic oscillator at 850 nm using a single-mode vcsel and a photonic crystal fiber. *IEEE Photonics Technology Letters*, 19(19), 1451-1453. <https://doi.org/10.1109/LPT.2007.903950>

Hayat, A., Varón, M., Bacou, A., Rissons, A., and Mollier, J. C. (2008, September 30 – October 3). 2.49 GHz low phase-noise optoelectronic oscillator using 1.55 $\mu\text{m}$  VCSEL for avionics and aerospace applications [Conference presentation]. 2008 IEEE International Meeting on Microwave Photonics, jointly held with the 2008 Asia-Pacific Microwave Photonics Conference, Gold Coast, Qld, Australia. <https://doi.org/10.1109/MWP.2008.4666644>

Iakovlev, V., Suruceanu, G., Caliman, A., Mereuta, A., Mircea, A., Berseth, C., Syrбу, A., Rudra, A., and Kapon, E. (2005). High-performance single-mode VCSELs in the 1310-nm wa-



- veband. *IEEE Photonics Technology Letters*, 17(5), 947-949. <https://doi.org/10.1109/LPT.2005.845654>
- IEEE (2009). *IEEE standard definitions of physical quantities for fundamental frequency and time metrology—random instabilities (IEEE Std 1139-2008)*. IEEE. <https://doi.org/10.1109/IEEESTD.2008.4797525>
- IEEE (2021). *Standard for jitter and phase noise (IEEE Std 2414-2020)*. IEEE.
- International Telecommunication Union (ITU) (1996). *ITU- T recommendation G.810 (08/96), definitions and terminology for synchronization networks*. ITU.
- International Telecommunication Union (ITU) (2018). *G.8251: The control of jitter and wander within the optical transport network (OTN)*. ITU.
- Koizumi, K., Yoshida, M., and Nakazawa, M. (2009). 10-GHz 11.5-ps pulse generation from a single-mode gain-switched InGaAs VCSEL at 1.1  $\mu\text{m}$ . *IEEE Photonics Technology Letters*, 21(22), 1704-1706. <https://doi.org/10.1109/LPT.2009.2031920>
- Koizumi, K., Yoshida, M., and Nakazawa, M. (2010). A 10-GHz optoelectronic oscillator at 1.1  $\mu\text{m}$  using a single-mode VCSEL and a photonic crystal fiber. *IEEE Photonics Technology Letters*, 22(5), 293-295. <https://doi.org/10.1109/LPT.2009.2038892>
- Lavrencik, J., Thomas, V.-A., Varughese, S., and Ralph, S.-E. (2017). DSP-enabled 100 Gb/s PAM-4 VCSEL MMF links. *Journal of Lightwave Technology*, 35(15), 3189-3196. <https://doi.org/10.1109/JLT.2017.2683941>
- Lu, H., Li, C., Chen, H., Ho, C., Cheng, M., Yang, Z., and Lu, C. (2017). A 56 Gb/s PAM4 VCSEL-based LiFi transmission with two-stage injection-locked technique. *IEEE Photonics Journal*, 9(1), 1-8. <https://doi.org/10.1109/JPHOT.2016.2637564>
- Malacarne, A., Fresi, F., Meloni, G., Foggi, T., and Poti, L. (2017). Time-frequency packing applied to cost-effective IM/DD transmission based on directly modulated VCSEL. *Journal of Lightwave Technology*, 35(20), 4384-4391. <https://doi.org/10.1109/JLT.2017.2743529>
- Park, M., Kwon, O., Han, W., Lee, K., Park, S., and Yoo, B. (2006). All-epitaxial InAlGaAs-InP VCSELs in the 1.3-1.6- $\mu\text{m}$  wavelength range for CWDM band applications. *IEEE Photonics Technology Letters*, 18(16), 1717-1719. <https://doi.org/10.1109/LPT.2006.879940>
- Pavan, S.-K., Lavrencik, J., and Ralph, S.-E. (2017). VCSEL-Based PAM-4 Links up to 62 Gbit/s over OM3, OM4, and WB-MMF: Performance Comparison at 850 nm and 1050 nm. *Journal of Lightwave Technology*, 35(9), 1614-1623. <https://doi.org/10.1109/JLT.2016.2647203>
- Rappaport, T. S., Xing, Y., Kanhere, O., Ju, S., Madanayake, A., Mandal, S., Alkhateeb, A., and Trichopoulos, G. C. (2019). wireless communications and applications above 100 GHz: Opportunities and Challenges for 6G and Beyond. *IEEE Access*, 7, 78729-78757. <https://doi.org/10.1109/ACCESS.2019.2921522>
- Rissons, A., Poulencard, S., Laurent, B., and Mollier, J. (2012, September 11-14). *Advances in VCSEL for satellite applications* [Conference presentation]. 2012 IEEE International Topical Meeting on Microwave Photonics, Noordwijk, Netherlands. <https://doi.org/10.1109/MWP.2012.6474110>
- Rubiola, E. (2008). *Phase noise and frequency stability in oscillators*. Cambridge University Press. <https://doi.org/10.1017/CBO9780511812798>
- Rubiola, E. and Giordano, V. (2007). On the 1/f frequency noise in ultra-stable quartz oscillators. *IEEE Transactions on Ultrasonics, Ferroelectrics, and Frequency Control*, 54(1), 15-22. <https://doi.org/10.1109/TUFFC.2007.207>
- Ryu, K., Lee, K.-H., Lim, J.-P., Kim, J., Pae, H., Park, J., Lim, H.-W., and Lee, J.-Y. (2020). An analytical jitter tolerance model for DLL-based clock and data recovery circuits. *IEEE Transactions on Very Large Scale Integration (VLSI) Systems*, 28(11), 2257-2267. <https://doi.org/10.1109/TVLSI.2020.3018794>
- Sung, H., Lau, E. K., Zhao, X., Parekh, D., Chang-Hasnain, C., and Wu, M. (2007, May 6-11). *Optically injection-locked optoelectronic oscillators with low RF threshold gain* [Conference presentation]. 2007 Conference on Lasers and Electro-Optics (CLEO), Baltimore, MD, USA. <https://doi.org/10.1109/CLEO.2007.4453176>
- Syrbu, A., Iakovlev, V., Suruceanu, G., Caliman, A., Mereuta, A., Mircea, A., Berseth, C.-A., Diechsel, E., Boucart, J., Rudra, A., and Kapon, E. (2005, January 22-27). *VCSELs emitting in the 1310-nm waveband for novel optical communication applications* [Conference presentation]. SPIE 5737, Vertical-Cavity Surface-Emitting Lasers IX, San José, CA, United States. <https://doi.org/10.1117/12.606964>
- Varón, M., Martín, J.-C., Le Kernec, A., and Mollier, C. (2006, October 2-4). *VCSEL based oscillator for harmonic frequency generation* [Conference presentation]. 5th Topical Meeting on Optoelectronic Distance/Displacement Measurements and Applications, Madrid, Spain.
- Wagner, C., Dochhan, A., Eiselt, M.-H., Grobe, K., Ortsiefer, M., Greus, C., Neumeier, C., Paul, S., Cesar, J., Kuppers, F., Olmos, J.-J.-V., and Monroy, I.-T. (2017). 26-GB/s DMT transmission using full C-band tunable VCSEL for converged PONs. *IEEE Photonics Technology Letters*, 29(17), 1475-1478. <https://doi.org/10.1109/LPT.2017.2710323>
- Wang, W., Liu, Y., Du, X., Zhong, X., Yu, C., and Chen, X. (2020). Ultra-stable and real-time demultiplexing system of strong fiber bragg grating sensors based on low-frequency optoelectronic oscillator. *Journal of Lightwave Technology*, 38(4), 981-988. <https://doi.org/10.1109/JLT.2019.2949682>
- Yao, X. S. and Maleki, L. (1996). Optoelectronic oscillator for photonic systems. *IEEE Journal of Quantum Electronics*, 32(7), 1141-1149. <https://doi.org/10.1109/3.517013>
- Zou, X., Liu, X., Li, W., Li, P., Pan, W., Yan, L., and Shao, L. (2016). Optoelectronic oscillators (OEOs) to sensing, measurement, and detection. *IEEE Journal of Quantum Electronics*, 52(1), 1-16. <https://doi.org/10.1109/JQE.2015.2504088>